Prediction of Fracture Stress with Regard to Porosity in Cast A356 Alloy

H. Sahin [a], M. Atik [a], F. Tezer [a], S. Temel [a], O. Aydin [a], O. Kesen [a], O. Gursoy [b], D. Dispinar [c, *]

[a] Istanbul Technical University, Turkey
[b] University of Padova, Italy
[a] Foseco, Netherlands
* Corresponding author. E-mail address: derya.dispinar@gmail.com

Abstract

Production of the defect-free casting of aluminium alloys is the biggest challenge. Porosity is known to be the most important defect. Therefore, many cast parts are subjected to several non-destructive tests in order to check their acceptability. There are several standards, yet, the acceptance limit of porosity size and distribution may change according to the customer design and requirements. In this work, the aim was targeted to evaluate the effect of size, location, and distribution of pores on the tensile properties of cast A356 alloy. ANSYS software was used to perform stress analysis where the pore sizes were changed between 0.05 mm to 3 mm by 0.05 mm increments. Additionally, pore number was changed from 1 to 5 where they were placed at different locations in the test bar. Finally, bifilms were placed inside the pore at different sizes and orientations. The stress generated along the pores was recorded and compared with the fracture stress of the A356 alloy. It was found that as the bifilm size was getting smaller, their effect on tensile properties was lowered. On the other hand, as bifilms were larger, their orientation became the dominant factor in determining the fracture.

Keywords: Casting defects, Mechanical properties, A356, Bifilm, porosity, Fracture stress

1. Introduction

Al-Si alloys are used in many industrial applications such as automotive and aerospace due to their corrosion resistance, fluidity, and high tensile strength to weight ratio. Porosity is known to be the most important factor that deteriorates the properties of aluminium alloys. There are several approaches in the literature about porosity sources in casting operations. Some claim that hydrogen solubility is an important factor. On the other hand, bifilm defects are known to be the major source of porosity since the folded oxide contains an air gap which is opened (i.e. unfurling) during solidification contraction to form the porosity.

Two types of pores are available in cast alloys: micro shrinkage and gas pore [1]. There are several works that show that hydrogen is not the main factor for porosity formation, but can be a contributor [2-6]. If the oxide formed on the surface is entrained into the liquid aluminium by turbulence (Figure 1) the dry sides of the oxide collide with each other and fold over and thereby trap the air inside.
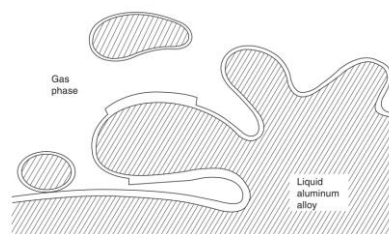

Fig. 1. Formation Mechanism of Bifilms [7]

These bifilms act like a crack in the liquid, a ceramic-ceramic unbound interface occurs and causes the casting part to fail under stress. This defect is also called a double oxide film. During solidification, the folded bifilms may unravel in the form of a flat crack (Figure 2). the porosity formation is enhanced by the opening of bifilms mainly by solid/liquid contraction. As a result, the pieces of the original bifilm oxide may end up fractured inside the pore cavity in between the dendrites.
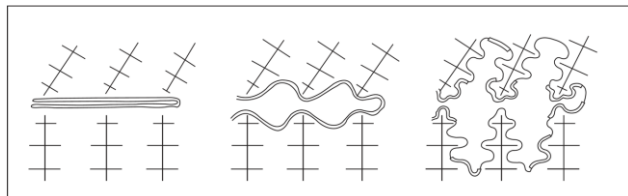

Fig. 2. Porosity formation by bifilms [7]

With this action, bifilms increase their harmful effects by ten times. This mechanism is defined as folding/unfolding and furling/unfurling [7]. These types of cracks can be suspended in liquid aluminium for a long time. The reason for this is that the density of the aluminium oxide is close to the density of the liquid aluminium. Additionally, they have an air gap in between the folded oxides. Therefore, they can float in the liquid and they would never sediment to the bottom; or float to the surface. Thus, the determination of the presence of these defects in the liquid aluminium prior to casting plays a critical role in order to achieve high-quality, defect-free castings.

Bifilm index [4] can be calculated as the sum of the maximum length of pores (L_b) on the cross-section of Reduced Pressure Test samples solidified under 100 mbar. The bifilm index range is defined as follows [8]:

0-25 mm: best quality
25-50 mm: good quality
50-100 mm: average quality
100-150 mm: bad quality
> 150 mm: don't cast!

Bifilms could not be detected for a long time because they were very thin. This problem was solved by a reduced pressure test. Solidification under vacuum helps the bifilms to open up. This test is used to detect invisible, thin but harmful bifilms. It works on the principle of expanding and making the bifilm observable by expanding the gas trapped between the bifilm in a partial vacuum environment. There are several works in the literature [9-36] on the effects of bifilms on different properties of cast aluminium alloys and how they can be removed from the casting process. The critical issue is the establishment of optimised degassing operation such that fine and small bubbles are generated to float the bifilms to the surface of the melt [33].

The effect of porosity on high pressure die casting was investigated [34]. The position and shape of the porosity were determined by a Computed Tomography Scan and fracture mechanics were examined. In this study, porosity was found to be the effective parameter on the fracture mechanics. At the same time, it was found that the shape of porosity was more effective on fracture mechanics than its size.

The fatigue effect of bifilm using the X-ray tomography method in A356 alloy was examined [36]. The results were analysed by the finite element method. They found that the position of the pores was important. In the finite element method, it was determined that pores create more stress than defect-free test samples.

The fracture micro-mechanism at room temperatures of the casting made by the lost foam method was studied [37]. The microstructure optimized by computed tomography scan with finite element method was analysed. The starting point of the cracks that initiated failure was found to be the pores.

In-situ fatigue test and 3-dimensional finite element analysis on A357-T6 alloy were performed [38]. The tomographic examination was performed with computed tomography -Scan for visualization of the internal defects. According to their findings, crack nucleation was found on pore surfaces.

The relationship between bifilm and pores in Al-Si-Mg-Cu based alloy [39] showed that a layer of aluminum oxide on the inner surfaces of the pores was present which revealed that the pores consist of bifilm.

The effect of micropores on the mechanical properties by X-ray tomography [40] showed that the fracture strain was decreased from 17 to 3 % with an increase in porosity content. In the case of the specimens that contain pores higher than 100 mm, the ultimate tensile strength was found to be decreased monotonically.

The finite element method is a numerical technique for solving problems that are defined by partial differential equations or can be formulated as functional minimization. In this current work, Ansys software that works on the finite element method principle [41] was used to evaluate the size, shape, and location of the pores with regard to the fracture stress that occurred in the tensile bars in A356 alloy. There has been a long-going discussion about the effect of pores on the mechanical properties of cast alloys. This work aims to contribute the effect of the presence of bifilms on tensile properties of A356 alloy with regard to their shape, size, location, and orientation along the force exerted upon the material.

2. Experimental work

In this study, A356, Table 1, was sand cast as 20 cylindrical bars (150 mm length and 10 mm diameter) at 730°C.

Table 1.
Chemical Composition of A356 Alloy (%wt.)

Alloy	Si	Fe	Cu	Mn	Zn	Ti	Al
A356	6.8	0.35	0.02	0.03	0.04	0.04	Bal.

After machining of the bars into the ASTM E8 standards, the test specimens were subjected to computed tomography Scan in YXLON MU-2000. After the tensile tests were completed, the fracture of the samples was correlated with the position and size of the pores.

For a detailed analysis of the effect of pores on the tensile properties, porosities of different sizes between 0.25-1 mm in diameter; and pore numbers ranging from 1 to 5 were placed in the tensile test specimen. These tensile test specimens were analysed by the finite element method using Ansys under

different loads from 5 MPa to 250 MPa. The material data was used from the Total Materia database.

A sample from the computed tomography scan analysis was taken and bifilm at different sizes and locations were placed in the pores. Ansys analysis was performed to investigate the stress generated along with the pores. For the effect of bifilms, young oxide (amorphous) and old oxide (γ-Al$_2$O$_3$) were defined in the Ansys analysis. Using the mechanical property database, the properties of two oxides were input as parameters to Ansys.

3. Results

In order to examine the effect of porosity on the fracture mechanics of the cast sample, pores with different sizes and numbers were placed in the tensile test specimen and stress analysis was performed with the Ansys program under different loads, Figure 3. As can be seen, when 75 MPa of stress is applied to the test bar, 129.44 MPa occurs around the pore (diameter 1 mm). These values are 168, 180, and 195 MPa for 100, 110, and 125 MPa, respectively. Considering that the yield stress of A356 is 140 MPa, it can be seen from Fig. 3. that in the existence of a 1 mm pore, 100 MPa of stress is good enough to reach the theoretical (defect-free) yield strength values.
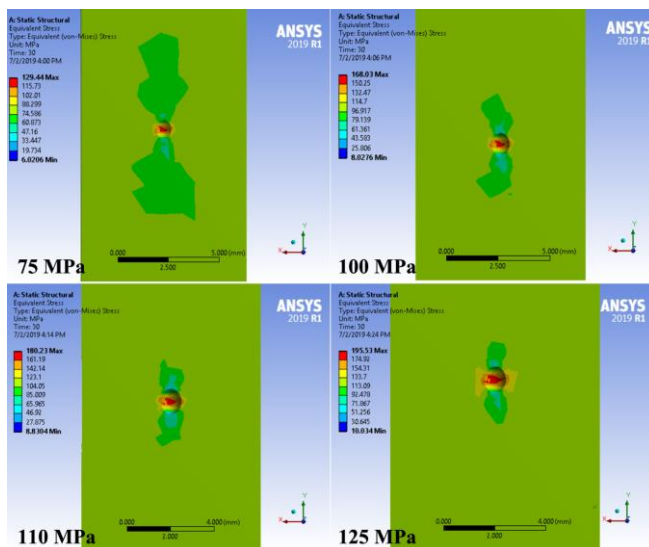

Fig. 3. Stress analysis of tensile bar with a single pore under different loads

A similar analysis was run for the test samples where there are five pores in the cast piece, Figure 4. When the pores have a radius of 0.5 mm, the stress values generated around the pores are 165.92, 179.11, 191.23, and 204.2 MPa for the loads applied at 90, 100, 110, and 125 MPa, respectively. From these calculations, it can be understood that 90 MPa is good enough to plastically deform the cast piece because the stress values reach the yield value of A356.

As mentioned in the experimental section, Ansys analysis were run for pores having radii changing between 0.25 to 1 mm with their number changing from 1 to 5. From all these test runs,

statistical analysis results were obtained, and thereby counter graphs were plotted. When the cross-section area of the pores along the tensile axis is considered, Figure 5, that the material can withstand the stress under yield point when the total area of pores is smaller than 1 mm^2. When the pore area is between 1 and 8 mm^2, it was found that the stress generated on the tensile sample was not significantly changing. However, the stress that occurred on the sample is dramatically increasing when pores are larger than 8 mm^2 and the stress applied to the sample is above 70 MPa.
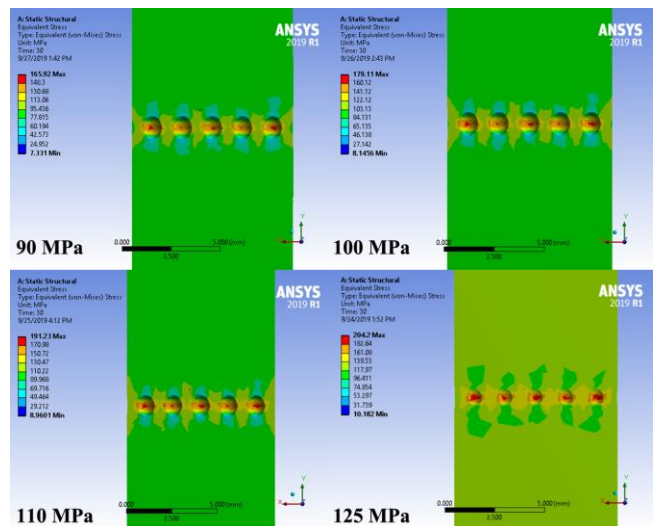

Fig. 4. Stress analysis of tensile bar with five pores under different loads

When the volume of the pores is considered, in Figure 6, there is a similar trend to that of the area, Figure 5. In samples with a pore volume of 1 mm^3, it is seen that it approaches the yield limit under 100 MPa load. When the pore volume is above 1 mm^3, the yield stress limit can be reached at 80 MPa load.
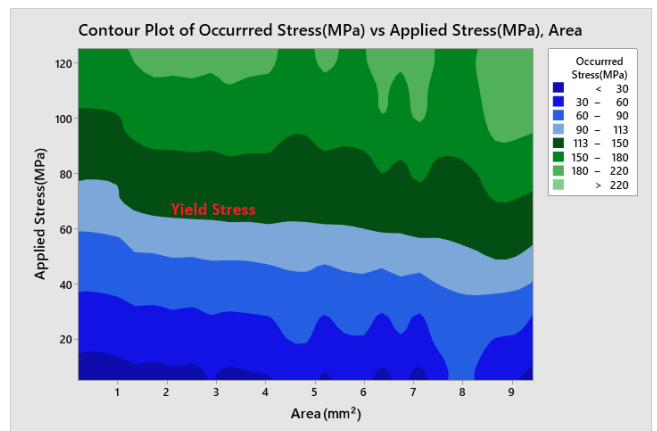

Fig. 5. Contour Plot of generated Stress vs Applied Stress per area of the pore

Ten cylindrical bars were machined to standards as given in Experimental Section. The samples were produced by casting into a sand mould where 10 bars were produced with diameter of 10

and height of 160 mm. They were then machined according to ASTEM E-8 standards. All samples were subjected to computed tomography Scan analysis, Figure 7. After the tests were complete, the fracture locations and the size of pores at the fracture point were recorded.

Based on the computed tomography results, Figure 7, bifilms were placed inside the pore with regard to the possible locations of the oxides, Figure 2. A matrix was formed where bifilms were located inside the pore, Figure 8. The placement of bifilms was chosen as:

A: complete bifilm: whole surface area inside the pore was considered as an oxide

B: half bifilm: only half of the pore's inner surface was oxide

C: quarter bifilm: 1/4th of the pore's inner surface was oxide

D: half of quarter bifilm: 1/8th of pore's inner surface was oxide

In addition to the size of the oxides inside the pores, their locations were also considered, Figure 9, where;

A1: complete bifilm: only one position (since the whole surface is oxide)

B1-6: left, right, top, bottom, front, back

C1-12: left-right, top-bottom, front-back and its combinations
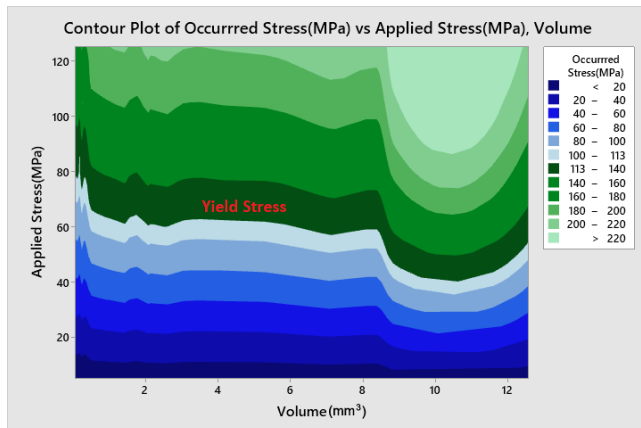
D1-8: left-right, top-bottom, front-back

Fig. 6. Contour Plot of generated Stress vs Applied Stress per volume of pore

The oxide structure depends on the formation mechanism. Young oxide is known as amorphous oxide with a thickness of approximately 200 nm. It is typically formed on the surface of the melt instantly. For example, after the removal of the skim on the surface, the shiny-looking oxide is amorphous which resembles a stretch film that is transparent. The old oxide is the thick and crystallized form of amorphous oxide, also known as γ-Al_2O_3.

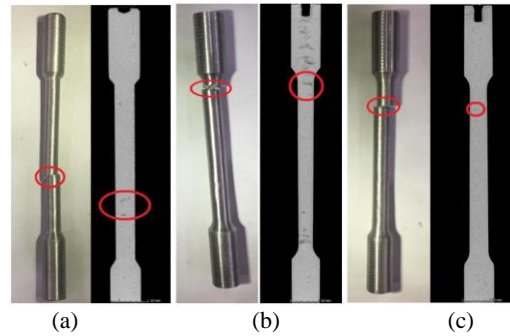(a)   (b)   (c)

Fig. 7. The breakpoints of tensile bars and CT Scan Analyses

An example of the stress generated on the pores according to the bifilm size and location shows a distribution of stress, Figure 5. When the whole inner surface of the pore is covered with oxide, the stress generated in the matrix of the alloy reaches 95.43 MPa while the stress on the oxide itself is around 817.5 MPa. In the case of the presence of half an oxide, Figure 10 c-d, the stress in the matrix becomes 136.6 MPa and 708.8 MPa on the oxide.
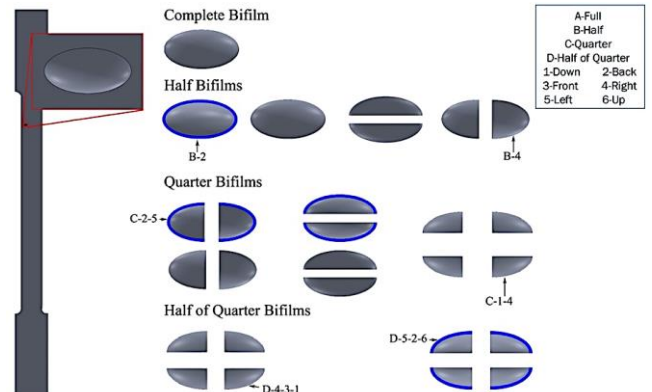

Fig. 8. Size and location of bifilms in the inner surface of a pore

A similar analysis was run for all the parameters, Figures 8 and 9. The findings of these data are summarised in Figure 11. According to finite element method analysis, it can be seen that the size and location of the oxide inside the pore have a dominant effect on the stress generated in the test bar. When the bifilm covers the whole surface of the pore, Figure 11, at a stress level of 60 MPa, the alloy reaches the yield point when the pore size is 0.7 mm. When half of the pore is covered with oxide (Fig. 11b) and the oxide is on the right of the pore (i.e. parallel to the tensile axis), 70 MPa of force is good enough to affect the alloy to reach yield; i.e. plastic deformation starts. On the other hand, when the oxide is placed at the bottom of the pore (i.e. perpendicular to the tensile axis), 30 MPa of force will lead to plastic deformation which is half the load needed when the oxide is parallel. Therefore, this result was the first indication that the orientation of bifilm along the tensile axis is important. The same scenario applies when a quarter of the pore is covered with oxide as seen in Fig. 11c. On the other hand, when the oxide is very small (as in the case of half of a quarter of pore is covered with bifilm, Figure 11d), the orientation of bifilm becomes irrelevant and the force applied does not affect the stress generated on the tensile bar.
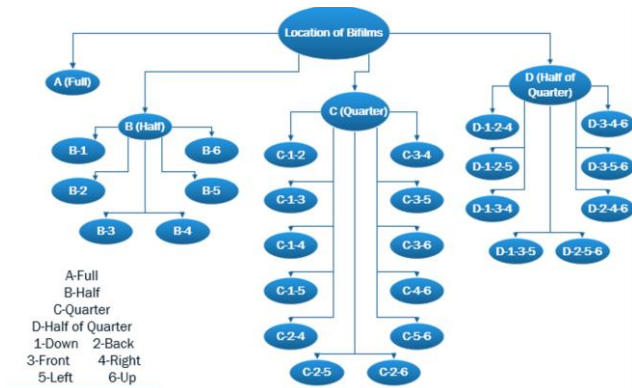
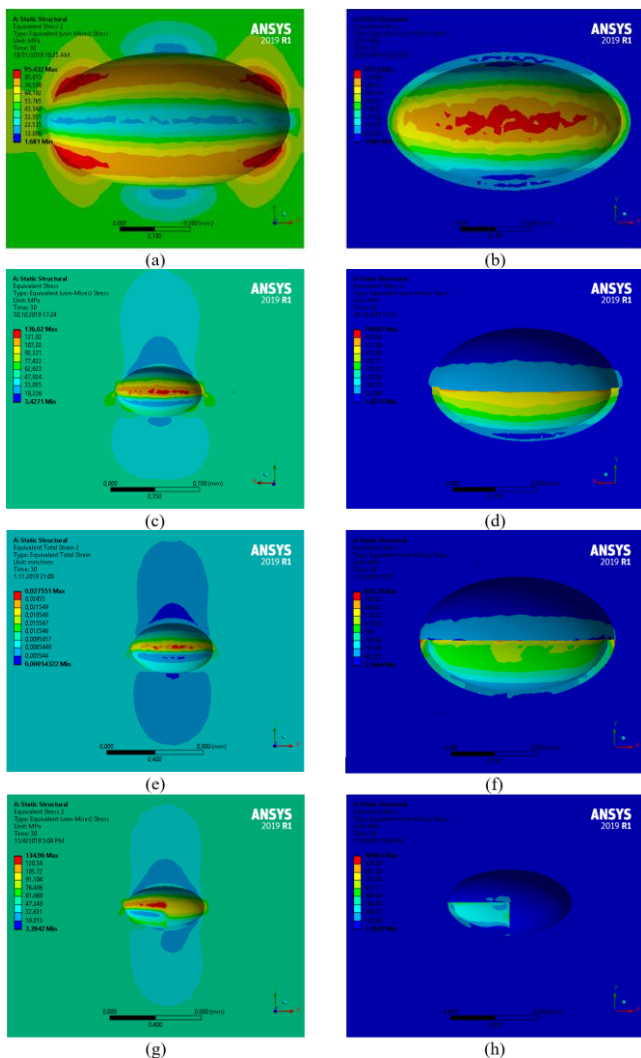Fig. 9. The coding of the location of bifilm inside the pores

Bifilms are oxides, and oxides can be in various thicknesses. Therefore, in order to determine the effect of thickness of the oxide on the same test parameters that have been carried out so far; all the tests were repeated for four different oxide thicknesses: 1, 5, 10, and 25 mm, Figure 12. When half of the inner surface of the pore is covered with oxide, Figure 12a., the stress generated in the tensile bar is the highest when the oxide is either on top to bottom of the pore. The effect of thickness of the oxide is so small, however, as expected, the thickest oxide always generated the highest stress towards the matrix. For the case when 1/4th of the inner surface is covered with oxide, Figure 12b, the effect of oxide thickness becomes more apparent: the higher the thickness, the higher the stress on the tensile bar. The lowest stress on the test bar is observed when the oxide is front and right of the pore. When 1/8th of the inner surface of the pore is covered with oxide, Figure 12c, the location of the oxide becomes irrelevant. The stress generated on the tensile bar is always the same regardless of the orientation of the oxide along the tensile axis. On the other hand, the effect of the thickness of the oxide becomes more dominant.
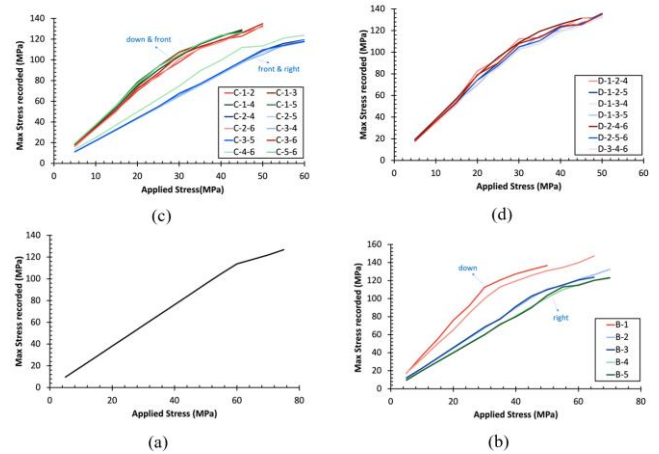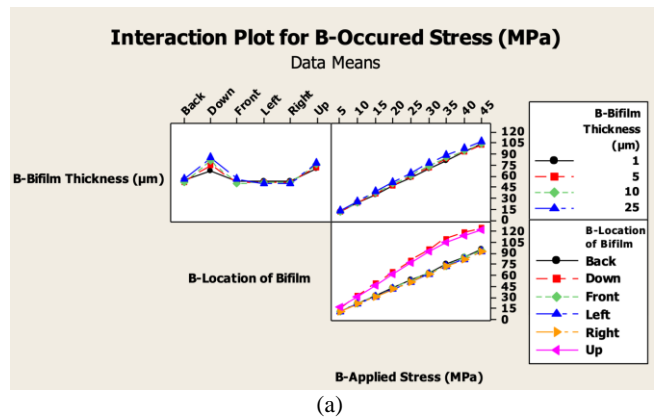

Fig. 11. Stress occurred on the samples with regard to size and position of bifilms
(a) complete bifilm, (b) half bifilm, (c) quarter bifilm, (d) half of quarter bifilm

Fig. 10. Stress generated on the matrix and the oxide for (a-b) complete bifilm, (c-d) half bifilm, (e-f) quarter bifilm, (g-h) half of quarter
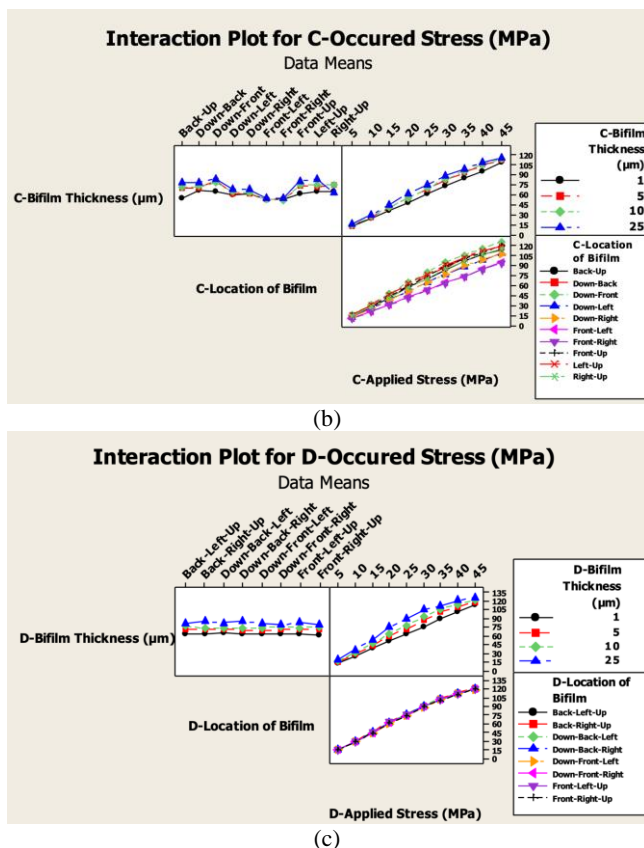

(a)

(b)

(c)

Fig. 12. Interaction plots showing the effect of bifilm thickness and orientation over the stress generated in the test bar in the presence of a pore (a) half, (b) quarter, (c) half of quarter of the inner surface of pore is an oxide

4. Conclusions

Porosity has a great influence on the mechanical properties of A356 alloy. The size, shape, and location of pores are the most important parameters that influence the fracture of cast A356.

There is a linear relationship between the size of pores and the tensile properties however when the number of pores increases, the relationship becomes more complex. When the volume of 1 pore and 5 pores is considered to be equal (i.e. one large and five small pores), the larger pore decreases the tensile properties more significantly than the small but five pores.

When bifilms are present in the pores, as the size of bifilm decreases, the effect on the mechanical properties decreases.

When bifilms cover more than half of the pores, their orientation along the tensile axis becomes important in terms of fracture. When they are located parallel to the tensile axis, the stress applied to the test bar generates less stress to the matrix.

An analytical approach was established between the pores' size and number with the mechanical properties. In this way, an estimation of the potential fracture stress can be determined just by looking into the computed tomography scan of a tensile bar and locating the size and number of pores.

References

[1] Buffiere, J.-Y., Savelli, S., Jouneau, P.-H., Maire, E. & Fougeres, R. (2001). Experimental study of porosity and its relation to fatigue mechanisms of model Al–Si7–Mg0. 3 cast Al alloys. *Materials Science and Engineering: A.* 316(1-2), 115-126. DOI: 10.1016/S0921-5093(01)01225-4.

[2] Dispinar, D. & Campbell, J. (2011). Porosity, hydrogen and bifilm content in Al alloy castings. *Materials Science and Engineering: A.* 528(10-11), 3860-3865. DOI: 10.1016/j.msea. 2011.01.084.

[3] Dispinar, D. & Campbell, J. (2004). Critical assessment of reduced pressure test. Part 1: Porosity phenomena. *International Journal of Cast Metals Research.* 17, 280-286. DOI: 10.1179/136404604225020696.

[4] Dispinar, D. & Campbell, J. (2004). Critical assessment of reduced pressure test. Part 2: Quantification. *International Journal of Cast Metals Research.* 17, 287-294. DOI: 10.1179/136404604225020704.

[5] Dispinar, D. & Campbell, J. (2006). Use of bifilm index as an assessment of liquid metal quality. *International Journal of Cast Metals Research.* 19, 5-17. DOI: 10.1179/ 136404606225023300.

[6] Dispinar, D. & Campbell, J. (2007). Effect of casting conditions on aluminium metal quality. *Journal of Materials Processing Technology.* 182, 405-410. DOI: 10.1016/j.jmatprotec.2006.08.021.

[7] Campbell, J. (2015). *Complete casting handbook: metal casting processes, metallurgy, techniques and design.* Butterworth-Heinemann.

[8] Dispinar, D. & Campbell, J. (2014). Reduced pressure test (RPT) for bifilm assessment. in *Shape Casting: 5th International Symposium 2014* 243-251.

[9] Asadian Nozari, M., Taghiabadi, R., Karimzadeh, M. & Ghoncheh, M. H. (2015). Investigation on beneficial effects of beryllium on entrained oxide films, mechanical properties and casting reliability of Fe-rich Al–Si cast alloy. *Materials Science and Technology.* 31, 506-512. DOI: 10.1179/1743284714Y.0000000656.

[10] Bagherpour-Torghabeh, H., Raiszadeh, R. & Doostmohammadi, H. (2017). Role of Mechanical Stirring of Al-Mg Melt in the Healing of Bifilm Defect. *Metallurigical and Materials Transactions B.* 48, 3174-3184. DOI: 10.1007/s11663-017-1067-9.

[11] Bjurenstedt, A., Seifeddine, S. & Jarfors, A. E. W. (2015). On the complexity of the relationship between microstructure and tensile properties in cast aluminum. *International Journal of Modern Physics B.* 29, 1540011. DOI: 10.1142/S0217979215400111.

[12] Bozchaloei, G. E., Varahram, N., Davami, P. & Kim, S. K. (2012). Effect of oxide bifilms on the mechanical properties of cast Al–7Si–0.3 Mg alloy and the roll of runner height after filter on their formation. *Materials Science and Engineering A.* 548, 99-105. DOI: 10.1016/j.msea. 2012.03.097.

[13] Çolak, M., Kayikci, R. & Dispinar, D. (2016). Melt cleanliness comparison of chlorine fluxing and ar degassing of secondary Al-4Cu. *Metallurgical and Materials*

Transactions B. 47, 2705-2709. DOI: 10.1007/s11663-016-0745-3.

[14] Davami, P., Kim, S. K. & Varahram, N. (2012). Effects of hydrogen and oxides on tensile properties of Al–Si–Mg cast alloys. *Materials Science and Engineering A.* 552, 36-47. DOI: 10.1016/j.msea.2012.04.111.

[15] Davami, P., Kim, S. K. & Tiryakioğlu, M. (2013). The effect of melt quality and filtering on the Weibull distributions of tensile properties in Al–7% Si–Mg alloy castings. *Materials Science and Engineering A.* 579, 64-70. DOI: 10.1016/j.msea.2013.05.014.

[16] Dispinar, D., Akhtar, S., Nordmark, A., Di Sabatino, M. & Arnberg, L. (2010). Degassing, hydrogen and porosity phenomena in A356. *Materials Science and Engineering A.* 527, 3719-3725. DOI: 10.1016/j.msea.2010.01.088.

[17] El-Sayed, M. A., Hassanin, H. & Essa, K. (2016). Bifilm defects and porosity in Al cast alloys. *The International Journal of Advanced Manufacturing Technology.* 86, 1173-1179. DOI: 10.1007/s00170-015-8240-6.

[18] El-Sayed, M. A., Hassanin, H. & Essa, K. (2016). Effect of casting practice on the reliability of Al cast alloys. *International Journal of Cast Metals Research.* 29, 350-354. DOI: 10.1080/13640461.2016.1145966.

[19] El-Sayed, M. A., Salem, H. A. G., Kandeil, A. Y. & Griffiths, W. D. (2014). Determination of the lifetime of a double-oxide film in al castings. *Metallurgical and Materials Transactions B.* 45, 1398-1406. DOI: 10.1007/s11663-014-0035-x.

[20] Erzi, E., Gürsoy, Ö., Yüksel, Ç., Colak, M. & Dispinar, D. (2019). Determination of acceptable quality limit for casting of A356 aluminium alloy: supplier's quality index (SQI). *Metals.* 9, 957. DOI: 10.3390/met9090957.

[21] Fiorese, E., Bonollo, F., Timelli, G., Arnberg, L. & Gariboldi, E. (2015). New classification of defects and imperfections for aluminum alloy castings. *International Journal of Metalcasting.* 9, 55-66. DOI: 10.1007/BF03355602.

[22] Gopalan, R. & Prabhu, N. K. (2011). Oxide bifilms in aluminium alloy castings–a review. *Materials Science and Technology.* 27, 1757-1769. DOI: 10.1179/1743284711Y.0000000033.

[23] Hsu, F.-Y., Jolly, M. R. & Campbell, J. (2007). The design of L-shaped runners for gravity casting. in *Metals & Materials Society The Minerals, Proceedings of Shape Casting: 2nd International Symposium, Orlando, FL, USA.*

[24] Kang, M. *et al.* (2014). Tensile properties and microstructures of investment complex shaped casting. *Materials Science and Technology.* 30, 1349-1353. DOI: 10.1179/1743284713Y.0000000444.

[25] Mostafaei, M., Ghobadi, M., Eisaabadi, G., Uludağ, M. & Tiryakioğlu, M. (2016). Evaluation of the effects of rotary degassing process variables on the quality of A357 aluminum alloy castings. *Metallurgical and Materials Transactions B.* 47, 3469-3475. DOI: 10.1007/s11663-016-0786-7.

[26] Puga, H., Barbosa, J., Azevedo, T., Ribeiro, S. & Alves, J. L. (2016). Low pressure sand casting of ultrasonically degassed AlSi7Mg0.3 alloy: modelling and experimental validation of

mould filling. *Materials and Design.* 94, 384-391. DOI: 10.1016/j.matdes.2016.01.059.

[27] Stefanescu, D. M. (2005). Computer simulation of shrinkage related defects in metal castings–a review. *International Journal of Cast Metals Research.* 18, 129-143. DOI: 10.1179/136404605225023018.

[28] Tiryakioğlu, M., Campbell, J. & Nyahumwa, C. (2011). Fracture surface facets and fatigue life potential of castings. *Metallurgical and Materials Transactions B.* 42, 1098-1103. DOI: 10.1007/s11663-011-9577-3.

[29] Tunçay, T. & Bayoğlu, S. (2017). The effect of iron content on microstructure and mechanical properties of A356 cast alloy. *Metallurgical and Materials Transactions B.* 48, 794-804. DOI: 10.1007/s11663-016-0909-1.

[30] Tunçay, T., Tekeli, S., Özyürek, D. & Dispinar, D. (2017). Microstructure–bifilm interaction and its relation with mechanical properties in A356. *International Journal of Cast Metals Research.* 30, 20-29. DOI: 10.1080/13640461.2016.1192826.

[31] Uludağ, M., Çetin, R., Dispinar, D. & Tiryakioğlu, M. (2017). Characterization of the Effect of Melt Treatments on Melt Quality in Al-7wt %Si-Mg Alloys. *Metals.* 7(5), 157. DOI:10.3390/met7050157.

[32] Uludağ, M., Çetin, R., Dişpinar, D. & Tiryakioğlu, M. (2018). On the interpretation of melt quality assessment of A356 aluminum alloy by the reduced pressure test: the bifilm index and its physical meaning. *International Journal of Metalcasting.* 12, 853–860. DOI:10.1007/s40962-018-0217-4.

[33] Yorulmaz, A., Erzi, E., Gursoy, O. & Dispinar, D. (2019). End product rejection rate and its correlation with melt treatment in direct-chill casted hot rolling slabs. *International Journal of Cast Metals Research.* 32, 164-170. DOI: 10.1080/13640461.2019.1598684.

[34] Zahedi, H. *et al.* (2007). The effect of Fe-rich intermetallics on the Weibull distribution of tensile properties in a cast Al-5 pct Si-3 pct Cu-1 pct Fe-0.3 pct Mg alloy. *Metallurgical and Materials Transactions A.* 38, 659-670. DOI: 10.1007/s11661-006-9068-3.

[35] Kuwazuru, O. *et al.* (2008). X-ray CT inspection for porosities and its effect on fatigue of die cast aluminium alloy. *Journal of Solid Mechanics and Materials Engineering.* 2(9), 1220-1231. DOI: 10.1299/jmmp.2.1220.

[36] Le, V.-D., Saintier, N., Morel, F., Bellett, D. & Osmond, P. (2018). Investigation of the effect of porosity on the high cycle fatigue behaviour of cast Al-Si alloy by X-ray micro-tomography. *International Journal of Fatigue.* 106, 24-37. DOI: 10.1016/j.ijfatigue.2017.09.012.

[37] Wang, L. *et al.* (2016). Influence of pores on crack initiation in monotonic tensile and cyclic loadings in lost foam casting A319 alloy by using 3D in-situ analysis. *Materials Science and Engineering A.* 673, 362-372. DOI: 10.1016/j.msea.2016.07.036.

[38] Vincent, M., Nadot-Martin, C., Nadot, Y. & Dragon, A. (2014). Fatigue from defect under multiaxial loading: efect Stress Gradient (DSG) approach using ellipsoidal Equivalent Inclusion Method. *International Journal of Fatigue.* 59, 176-187. DOI: 10.1016/j.ijfatigue.2013.08.027.

[39] Gyarmati, G., Fegyverneki, G., Mende, T. & Tokár, M. (2019). Characterization of the double oxide film content of liquid aluminum alloys by computed tomography. *Materials Characterization.* 157, 109925. DOI: 10.1016/j.matchar. 2019.109925.

[40] Kobayashi, M., Dorce, Y., Toda, H. & Horikawa, H. (2010). Effect of local volume fraction of microporosity on tensile properties in Al–Si–Mg cast alloy. *Materials Science and Technology.* 26, 962-967. DOI: 10.1179/174328409X 441283.

[41] Nikishkov, G. P. (2004). Introduction to the finite element method. *Univ. Aizu* 1-70.